Full-Parameter Identification of Buck Converter Through BP-NN Fitting Explicit Time-Domain Relationships

Zhennan She, Yisi Liu, Wen Cao, and Guipeng Chen

***Abstract*—In this article, a backpropagation neural network (BP-NN) is employed to identify all component parameters of the Buck converter by fitting the explicit time-domain relationships. Thanks to the powerful ability to fit the nonlinear relationship of BP-NN, the proposed method can effectively avoid a large amount of direct calculation and thus it is convenient to implement. Meanwhile, the explicit time-domain relationships between voltage/current and component parameters in the Buck converter are revealed and utilized to train BP-NN. Hence, higher parameter identification accuracy and lower network configuration requirements are favorably achieved in comparison with the conventional NN-based method with ambiguous relationships. Besides, the proposed method is also experimentally validated on a closed-loop Buck converter. It is not only workable under different operating conditions, but also is effective in monitoring parameter variation during the component aging process.**

***Index Terms*—Buck converter, full-parameter identification, neural network (NN), time domain.**

I. Introduction

IN MANY mission-critical applications, such as aerospace, electric transportation, and data centers [1], [2], [3], the reliability of switching mode power supplies (SMPS) is extra important. Once the SMPS fails, personal safety and economic production will be seriously endangered. According to the research work in [4] and [5], component aging is one of the most important reasons for the failure of SMPS, which is thereby essential to monitor. Generally, the aging condition of components in SMPS such as capacitors, switches, inductors, and diodes, can be predicted by the values of their intrinsic parameters. For example, as a capacitor degrades, its capacitance decreases while its equivalent series resistance (ESR) increases. Similarly, the ON-state resistance of MOSFET, the inductance and its parasitic resistance of the inductor, and the forward voltage of the diode will vary as they age [6], [7]. To acquire the values of these health indicators of components, a lot of research has already been conducted, which can be mainly classified into two categories: single component individual identification [8], [9], [10], [11], [12], [13] and multiple components simultaneous identification [14], [15], [16], [17], [18], [19], [20], [21], [22], [23], [24], [25], [26], [27], as summarized in Fig. 1.

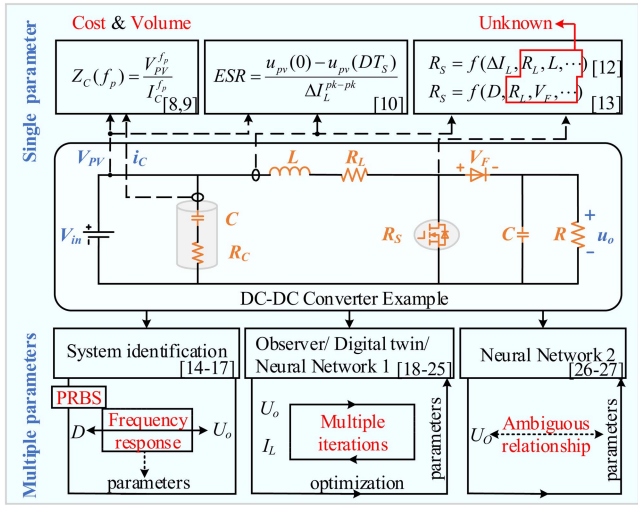

Fig. 1. Component parameter identification methods of DC–DC converters.

For a specific component, the most intuitive method to acquire its intrinsic parameter is to measure its voltage/current and then calculate directly. In [8], the ESR of the capacitor is approximately calculated by dividing its voltage at a high frequency by the current at the same frequency. Then, the capacitance can be approximately obtained from its voltage/current at a low frequency according to the research work in [9]. Nevertheless, additional sensors or measuring circuits are usually required, which increase the cost and volume of the system, especially when there are multiple components to be monitored. To avoid this shortcoming, the ESR of the input capacitor in the Boost converter is derived as a function of the input voltage in [10], and the capacitance of dc link is derived as a function of the dc-link

Manuscript received 2 June 2023; revised 27 October 2023 and 8 January 2024; accepted 18 February 2024. Date of publication 27 February 2024; date of current version 19 April 2024. This work was supported in part by the Fundamental Research Funds for the Central Universities under Grant 20720220083 and in part by Guangdong Basic and Applied Basic Research Foundation under Grant 2022A1515011616. Recommended for publication by Associate Editor L. Corradini. *(Corresponding author: Guipeng Chen.)*

Zhennan She and Wen Cao are with the School of Aerospace Engineering, Xiamen University, Xiamen 361102, China (e-mail: 35120211151612@stu.xmu.edu.cn; 35120231151750@stu.xmu.edu.cn).

Yisi Liu is with the Electrical Energy Management Group Laboratory, Department of Electrical and Electronic Engineering, University of Bristol, BS8 1TH Bristol, U.K. (e-mail: yisi.liu@bristol.ac.uk).

Guipeng Chen is with the School of Aerospace Engineering, Xiamen University, Xiamen 361102, China, and also with the Shenzhen Research Institute, Xiamen University, Shenzhen 518000, China (e-mail: cgp2017@xmu.edu.cn).

Color versions of one or more figures in this article are available at https://doi.org/10.1109/TPEL.2024.3370104.

Digital Object Identifier 10.1109/TPEL.2024.3370104

voltage in [11], which is already sampled for the control purpose. Moreover, Peng and Wang [12] derived the relationship between the ON-state resistance of MOSFET R_s and the duty cycle for Buck converter from the volt–second balance principle. Besides, Dusmez et al. [13] calculated R_s by analyzing and evaluating the variation in the plant model transfer function at double pole frequency. However, these calculations either are available for only one component or contain other component parameters that also need to be monitored.

Practically, compared with the single component individual identification, the multiple components' simultaneous identification is much expected in engineering applications. In [14], [15], [16], and [17], the system identification methods based on frequency domain are proposed. First, the pseudorandom binary sequence (PRBS) is injected into the controller to generate the corresponding excitation signal for the output voltage. Second, the transfer function of the output voltage and the duty cycle is established, and then the coefficients in the transfer function are obtained, to further calculate the multiple components parameters. Nevertheless, this method needs to derive the transfer function model, and it is also complex to identify the coefficients in the transfer function since the corresponding responses of different frequencies need to be extracted. Besides, the injection of PRBS will be detrimental to the stability of the system.

Different from the frequency domain, comprehensive condition monitoring from the time domain can avoid the undesired extra injected perturbation and the complex acquisition of frequency response [18], [19], [20], [21], [22], [23], [24], [25]. First, a virtual model mapped to the physical converter is constructed, e.g., observer in [18] and [19], digital twin in [20], [21], [22], and [23], and [24] and neural network (NN) in [25]. Then, an objective function is set for the consistency of voltage/current between the virtual model and the physical converter. Finally, the component parameters in the virtual model are searched by intelligent algorithms to complete identification. In [18] and [19], the observer uses the state equation to approximately calculate the observation values of each cycle. The adaptive algorithm is used to continuously update the observer coefficient to minimize the observation error until component parameters (capacitance and inductance) are identified. It takes a short time and the identification process can be implemented in the controller. However, the observer method generally ignores the parasitic parameters of components, because the complex model not only increases the difficulty of constructing the observer but also affects the speed and accuracy of parameter identification. To identify parasitic parameters besides the capacitance and inductance, a more accurate time-domain mathematical model of the converter is established in [20], [21], [22], [23], and [24]. In [20] and [21], the state space model including parasitic parameters is established and approximately solved by the Runge–Kutta algorithm to obtain the relationship from multiple component parameters to voltage/current. Then, the parameters are updated iteratively according to the minimum error of the voltage/current in multiple periods between the digital twin and the physical converter. Because the establishment of the digital replica requires complex mathematical derivation, the authors in [22], [23], and [24] used the simulation model of the converter built in Simulink/MATLAB to obtain data. However, each iteration process requires the simulation model to be recompiled, and thus it takes a long time. Similar to the research work in [20] and [21], the work in [25] also used the Runge–Kutta algorithm to solve the state space model with parasitic parameters, which in turn derives the equations between the initial/final and intermediate states of the voltage and current. Finally, multiple parameters are identified based on these state values. Since the intermediate state is unknown, the deep NN is used to construct and predict it, and the obtained result is used as a priori information for subsequent physical models. The method exploits the powerful universal approximation capability of the NN to construct intermediate states, which avoids additional computation. However, the derivation process of the physical model is also unavoidable. Besides, since the intermediate states are determined by the initial/ending states and the observable states are inconsistent each time, the intermediate variables need to be retrained by the network continuously.

Different from fitting the intermediate state in [25], the research work in [28] used the NN to train a fixed functional relationship. In [28], an NN is employed to build an emulator, which can reproduce the converter's dynamic behavior with great accuracy, and it is not focused on parameter identification. To apply NNs to parameter identification more effectively, the NN is employed in [26] and [27] to fit the relationship between voltages/ current and component parameters. In [26], multiple harmonic components of voltage/current are extracted first. Then, the harmonics and component parameters are used for the input and output of the NN. Further in [27], the frequency domain features and time domain statistical features of the output voltage are extracted and key features are further selected from them. Afterward, the relationship between selected key features and multiple component parameters is trained by an NN. Finally, the NN is employed to quickly identify the component parameters according to the sampled voltages during converter operation. In comparison with the virtual model method in [19], [20], [21], [22], [23], and [24], the NN-based parameter identification method is attractive that it effectively avoids constructing the mathematical model of the physical converter and iteratively searching the optimal parameters. However, there is no explicit physical relationship between the selected parameters in the existing methods. As a result, the NN based on ambiguous relations limits the accuracy of parameter identification results. In addition, the acquisition of these features requires high sampling rates and complex processing, which increases the implementation complexity.

To improve the accuracy and simplify the implementation, this article proposes a full-parameter identification method for Buck converter based on backpropagation NN (BP-NN) with explicit time-domain relationships, as shown in Fig. 2. First, the explicit relationships between the component parameters $\{R, L, C, R_C, R_L, R_S, V_F\}$ and the output voltage u_o/inductor current i_L in Buck converter are revealed. Then, the relationships are fitted by BP-NNs, which effectively avoid the large amount of calculation caused by directly solving component parameters from the relationships. Finally, the trained BP-NNs are further improved with the consideration of practical sampling noise, which are

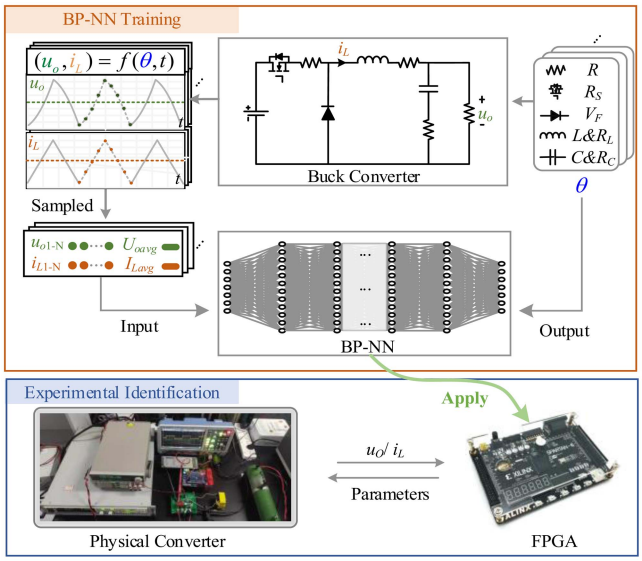

Fig. 2. Proposed full-parameter identification method through BP-NN fitting explicit time-domain relationships.

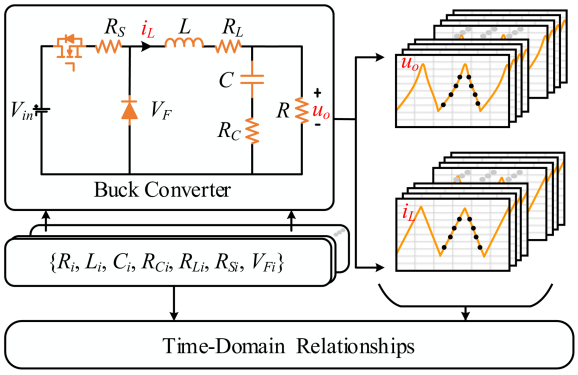

Fig. 3. Time-domain relationships in Buck converter.

then applied to the field-programmable gate array (FPGA) to identify all components' parameters of the physical converter during operation from the sampled data. Thanks to the explicit time-domain relationship, the parameter identification accuracy is high. Meanwhile, a small number of output voltage/inductor current data in a switching period is required and no additional processing is needed, hence the proposed method is also simple to implement.

The rest of this article is organized as follows. Section II reveals the explicit instantaneous and average time-domain relationships in the Buck converter. Subsequently, two BP-NNs are constructed to fit the instantaneous and average time-domain relationships to identify the full parameters of the Buck converter in Section III. In Section IV, an experimental closed-loop prototype is set up to verify the effectiveness of the proposed method. Finally, Section V concludes this article.

II. Explicit Time-Domain Relationships of Component Parameters to Voltage/Current

In Buck converter, as shown in Fig. 3, with different sets of component parameters, including the ON-state resistance of

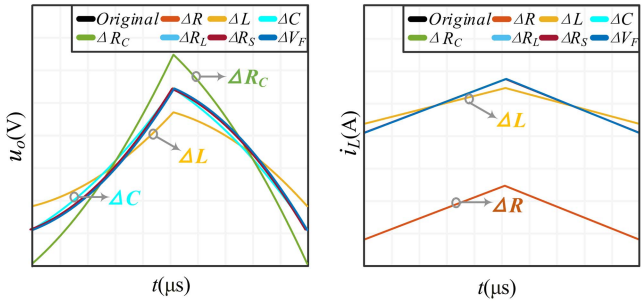

Fig. 4. Simulated results of output voltage and inductor current with change on different component parameters.

MOSFET R_S, the capacitance of output capacitor C and its ESR R_C, the inductance L and its parasitic resistance R_L, the load resistance R, and the diode forward voltage V_F, waveforms of steady-state output voltage u_o and inductor current i_L vary correspondingly. In fact, there are one-to-one explicit time-domain relationships between them, and they can be utilized to implement the parameters identification accurately and conveniently.

A. Instantaneous Time-Domain Relationship

For Buck converter, the instantaneous values of the output voltage u_o/inductor current i_L can be solved from its state space equations in (1), where $S = 1$ represents the switch is ON and $S = 0$ represents the switch is OFF. After considering all parasitic parameters of components, detailed expression of u_o and i_L will be very complex and hence it is simplified in (2). Theoretically, all component parameters $\{R, L, C, R_C, R_L, R_S, V_F\}$ have an impact on the instantaneous values of output voltage u_o and inductor current i_L, and their relationship is explicit. Nevertheless, their influences are different. As illustrated in Fig. 4, assuming that each parameter changes by 50% of the original value to obtain a clear view, parameters $\{R, L, C, R_C\}$ significantly affect the steady-state waveforms of output voltage u_o and inductor current i_L, whereas parameters $\{R_L, R_S, V_F\}$ have negligible effect. Furthermore, taking parameters L and R_L as an example, Fig. 5 shows their influences on u_o and i_L. It can be easily found in Fig. 5(a), once L changes by 5%, u_o and i_L vary accordingly

$$\begin{bmatrix} \frac{di_L}{dt} \\ \frac{dv_C}{dt} \\ v_O \end{bmatrix} = \begin{bmatrix} -\frac{1}{L}\left(R_L+SR_S+\frac{R_C R}{R_C+R}\right) & -\frac{1}{L}\left(\frac{R}{R_C+R}\right) \\ \frac{1}{C}\left(\frac{R}{R_C+R}\right) & -\frac{1}{C}\left(\frac{1}{R_C+R}\right) \\ \frac{R_C R}{R_C+R} & \frac{R}{R_C+R} \end{bmatrix} \times \begin{bmatrix} i_L \\ v_C \end{bmatrix} + \frac{S}{L}\begin{bmatrix} V_{in} \\ 0 \\ 0 \end{bmatrix} - \frac{(1-S)}{L}\begin{bmatrix} V_F \\ 0 \\ 0 \end{bmatrix} \tag{1}$$

$$(u_o, i_L) = f(R, L, C, R_C, R_L, R_S, V_F, t). \tag{2}$$

The same phenomenon can be seen in parameters R, C, and R_C. On the other hand, when R_L increases similarly by 5% in turn in Fig. 5(b), waveforms of u_o and i_L are almost overlapped and their instantaneous values are basically unchanged. The main

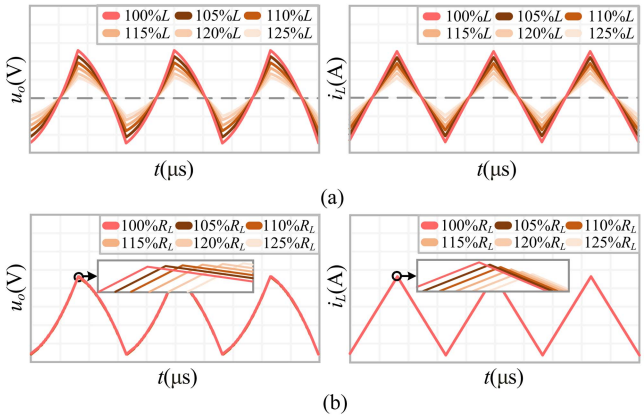

Fig. 5. Simulated results of output voltage and inductor current with successive 5% variation on different component parameters. (a) Inductance L. (b) Parasitic resistance of inductor R_L.

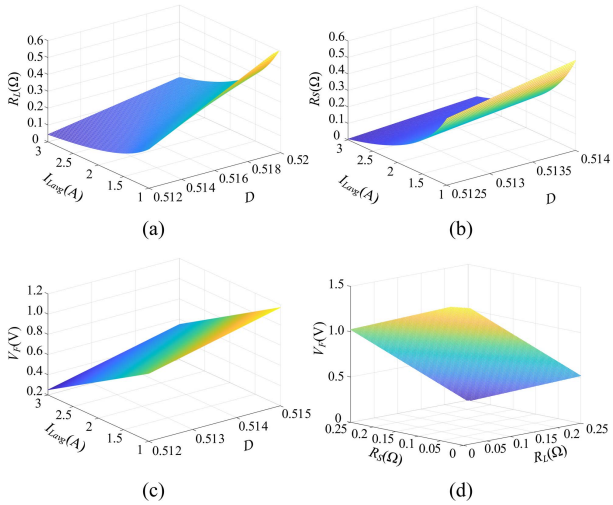

Fig. 6. Relationship between parameters (a) R_L, (b) R_S, (c) V_F, and duty cycle D under different I_{Lavg} operating conditions. (d) Relationship among three parameters $\{R_L, R_S, V_F\}$.

reason is that R_L is in series with L, and its voltage is much smaller than that of L. Likewise, R_S and V_F are also equivalent as in series with L when the switch is turned ON and OFF. Hence, their influences on u_o and i_L are also very small.

In conclusion, there is an explicit relationship between parameters $\{R, L, C, R_C\}$ and instantaneous values of u_o and i_L, whereas parameters $\{R_L, R_S, V_F\}$ have a weak relationship. Therefore, the instantaneous relationship can be employed to explicitly identify parameters $\{R, L, C, R_C\}$, but the identification of parameters $\{R_L, R_S, V_F\}$ requires another explicit relationship.

B. Average Time-Domain Relationship

As discussed earlier, the weak instantaneous relationship between parameters $\{R_L, R_S, V_F\}$ and u_o and i_L is caused by the influence of inductor L due to their series connection. According to the volt–second balance of the inductor, its average voltage in a steady-state period is zero. Therefore, the average time-domain relationship of the Buck converter in the following equation can be employed to avoid the undesired influence:

$$I_{Lavg} \times (R_L + D \times R_S) + (1 - D) \times V_F = D \times V_{in} - U_{oavg}. \quad (3)$$

From (3), parameters $\{R_L, R_S, V_F\}$ are highly correlated with the average values U_{oavg} and I_{Lavg} of output voltage, inductor current, the input voltage V_{in}, and duty cycle D. For most applications, U_{oavg} usually remains unchanged under the PI control. In addition, the relationships between D, I_{Lavg}, and $\{R_L, R_S, V_F\}$ are analyzed in Fig. 6 according to (3), respectively. In Fig. 6(a)–(c), the aging of $\{R_L, R_S, V_F\}$ causes the duty cycle D to increase under different I_{Lavg} operating conditions. Similarly, the aging of $\{R_L, R_S, V_F\}$ will also result in an increase in D under different V_{in} operating conditions and it is not repeatedly shown here. Furthermore, the relationship among parameters $\{R_L, R_S, V_F\}$ under a fixed operating condition is shown in Fig. 6(d). The relationship among $\{R_L, R_S, V_F\}$ is monotonically and uniquely mapped, so $\{R_L, R_S, V_F\}$ can be decoupled. In conclusion, there is an explicit relationship between parameters $\{R_L, R_S, V_F\}$ and $\{U_{oavg}, I_{Lavg}, D, V_{in}\}$. Therefore, the average relationship can be employed to explicitly identify parameters $\{R_L, R_S, V_F\}$.

III. Full-Parameter Identification Based on BP-NN

According to (2) and (3), if multiple instantaneous values of u_o and i_L in a steady-state period and multiple different sets of $\{U_{oavg}, I_{Lavg}, D, V_{in}\}$ under various operating conditions are provided, values of $\{R, L, C, R_C\}$ and $\{R_L, R_S, V_F\}$ can be calculated directly. However, the calculation involves a large number of complex operations, which is difficult to implement on digital processing chips. Fortunately, BP-NN is a powerful tool to approximate any relationship [29], [30] and is easy to implement on digital processing chips to perform the calculation quickly. Therefore, BP-NNs are used here to fit the aforementioned time-domain relationships (2) and (3) for the whole component parameters identification of the Buck converter. Compared with the research in [26] and [27], the BP-NNs are trained based on explicit physical relationships, hence the proposed method has high identification accuracy and does not require additional complex data processing. In this section, the overall BP-NN training scheme is demonstrated, along with the introduction of training data collection. In addition, the configuration design of BP-NNs is also discussed in detail to gain a favorable performance.

A. Overall BP-NN Training Scheme

The overall BP-NN training scheme for full-parameter identification of Buck converter based on explicit time-domain relationships is shown in Fig. 7. First, N sets of parameters $\{R_i, L_i, C_i, R_{Ci}, R_{Li}, R_{Si}, V_{Fi}, V_{ini}\}$ $(i = 1, 2, \ldots, N)$ are set, and then the "sim" function of MATLAB/Simulink is called to automatically obtain the waveforms of output voltage and inductor current for each parameter setting, instead of solving from (2) for simplicity. These waveforms are then processed to obtain the instantaneous and average values. Finally, the first

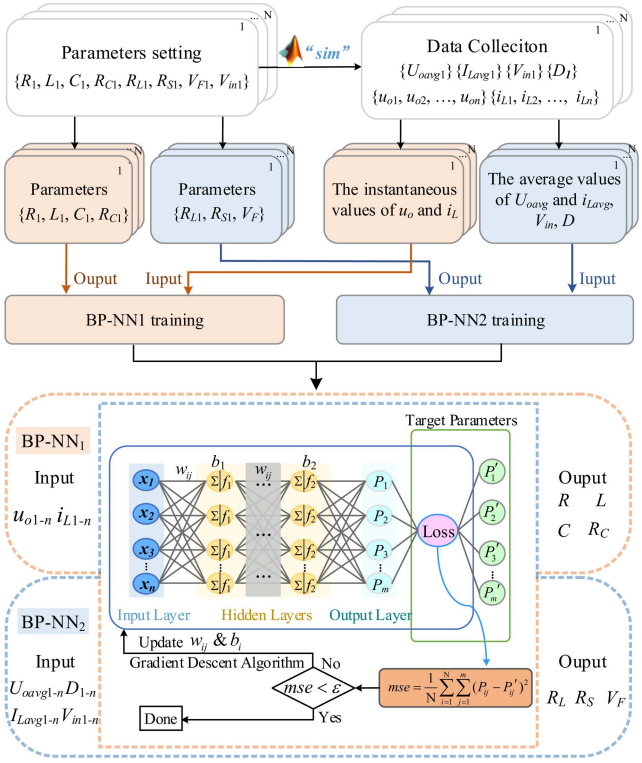

Fig. 7. Overall BP-NN training scheme for full-parameter identification of Buck converter based on explicit time-domain relationships.

NN BP-NN1 is established to fit the instantaneous time-domain relationship, whereas the second NN BP-NN2 is established to fit the average time-domain relationship. For BP-NN1, its inputs include several instantaneous values of output voltage (u_{o1}, u_{o2},. . ., u_{on}) and inductor current (i_{L1}, i_{L2},. . ., i_{Ln}) sampled in a switching period. The outputs are the parameters $\{R, L, C, R_C\}$. In addition, the inputs of BP-NN2 include several average values of output voltage (U_{oavg1}, U_{oavg2},. . ., U_{oavgn}) and inductor current (I_{Lavg1}, I_{Lavg2},. . ., I_{Lavgn}), the duty cycle (D_1, D_2,. . ., D_n), and the input voltages (V_{in1}, V_{in2},. . . V_{inn}) under different operation conditions. The outputs of BP-NN2 are the parameters $\{R_L, R_S, V_F\}$.

From Fig. 7, each BP-NN is composed of several layers, namely input layer, multiple hidden layers, and output layer. In addition, the hidden layers contain multiple nonlinear layers and a linear layer, and their activation functions f_1 and f_2 used here are "tansig(x) $= \frac{2}{1+e^{-2x}} - 1$" and "purelin($x$) $= x$," respectively. The values of each hidden layer are calculated by the input of the previous layer and weights w/biases b and activated nonlinearly or linearly by f_1 or f_2, which can approximate the complex nonlinear/linear operations in the time-domain relationships. Through multiple forward calculations, the training parameters (P_1, P_2,. . ., P_m) of the output layer are represented as functions of $u_{o1\text{-}n}$, $i_{L1\text{-}n}$ or $U_{oavg1\text{-}n}$, $i_{Lavg1\text{-}n}$, $D_{1\text{-}n}$, $V_{in1\text{-}n}$ with respect to w/b. To measure the degree of difference between the training parameters (P_1, P_2,. . ., P_m) and the target parameters (P_1', P_2',. . ., P_m'), the loss function of BP-NN is defined as the mean square error (MSE) between them, as shown in (4). If the loss

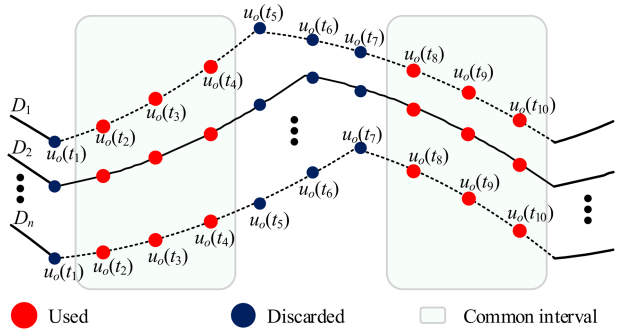

Fig. 8. Sampling strategy of instantaneous values at different duty cycles under fixed frequency control.

function is greater than the threshold ε, the gradient descent algorithm is used to minimize the loss function by reversely updating w and b in the hidden layers. After repeated training, once the loss function is less than ε, BP-NN training stops. At this time, the two trained BP-NNs can be employed to quickly identify full parameters $\{R, L, C, R_C, R_L, R_S, V_F\}$ from the new sampled data, so that the health status of the Buck converter can be conveniently monitored.

$$\text{MES} = \frac{1}{N}\sum_{i=1}^{N}\sum_{j=1}^{m}(P_{ij} - P_{ij}')^2 \tag{4}$$

where N represents the number of training data, and m represents the number of parameters participating in NN training.

B. Training Data Collection

To effectively train BP-NN, training data is very important. The number of training data for BP-NN typically ranges from several hundred to several million. Nevertheless, in power electronic converter applications, obtaining a large amount of training data from physical converters is difficult. To improve the simplicity of the proposed method, training data for both two BP-NNs are generated by the simulation results here, which are automatically obtained by computer.

For BP-NN1, the training data are obtained as follows. First, a closed-loop Buck converter model is established in Simulink/MATLAB. Subsequently, N groups of arbitrary parameters $\{R_i, L_i, C_i, R_{Ci}, R_{Li}, R_{Si}, V_{Fi}, V_{ini}\}$ ($i = 1, 2,. . ., N$) chosen from their minimum/maximum range are set to simulate the operation of the converter under different operating conditions. It can be easily implemented by repeatedly calling the "sim" function. As a result, N groups of output voltage/inductor current steady-state waveforms can be automatically obtained. For the fixed frequency control, ten data points will be sampled in a switching period, and the data points near the switching operation (ON or OFF of the switch) will be discarded since there will be severe interference noise. Because the turn-ON point under different duty cycle is constant, $u_o(t_1)$ will be discarded in all conditions, as shown in Fig. 8. On the other hand, the turn-OFF time varies under duty cycle 0.4–0.65 in this article, hence data points $u_o(t_5)$–$u_o(t_7)$ are also discarded because one of them

TABLE I
RANGE OF PARAMETER SETTINGS

Parameter / value	V_{in} (V)	R (Ω)	L (μH)	C (μF)	R_C (Ω)	R_L (Ω)	R_S (Ω)	V_F (V)	U_o (V)	f_{sw} (kHz)
Maximum	38	17	1800	130	0.48	0.65	0.6	0.7	24	20
Minimum	66	7	1400	95	0.02	0.15	0.1	0.5		

will be near the switching operation. For the variable frequency control with constant-on-time, the switch will also be turned on at the same point while its turn-OFF point is variable. In this case, $u_o(t_1)$ near the turn-ON point will also similarly be discarded in all conditions and other data points during the switch-ON interval will be used. Since the turn-OFF time is variable, the data points in the common area will be sampled during the switch-OFF interval.

Thus, under fixed-frequency control, only six points of voltage in a switching period waveform in a common interval are used as the training data. The same sampling strategy is used for i_L. For BP-NN1, each set of training data includes six instantaneous values of u_o and i_L, as well as corresponding parameters $\{R, L, C, R_C\}$.

For BP-NN2, the training data collection process is a little different. Because the identification of $\{R_L, R_S, V_F\}$ require multiple average values of output voltage ($U_{o\text{avg}1}, U_{o\text{avg}2},\ldots, U_{o\text{avg}n}$), inductor current ($I_{L\text{avg}1}, I_{L\text{avg}2},\ldots, I_{L\text{avg}n}$), duty cycle ($D_1, D_2,\ldots, D_n$), and input voltage ($V_{\text{in}1}, V_{\text{in}2},\ldots, V_{\text{in}n}$) under different operation conditions. Therefore, the aforementioned N groups of arbitrary parameters $\{R_i, L_i, C_i, R_{Ci}, R_{Li}, R_{Si}, V_{Fi}, V_{\text{in}i}\}$ ($i = 1, 2,\ldots, N$) are expanded by nine times, resulting in a total of $N * 9$ groups. For any $i * 9$ ($i = 1, 2,\ldots, N$) groups of parameters, $\{R_L, R_S, V_F\}$ remain the same, whereas the other parameters are arbitrarily set within the specified range. After that, the corresponding waveforms are automatically run by the Simulink to obtain $\{U_{o\text{avg}}, I_{L\text{avg}}, D, V_{\text{in}}\}$. For BP-NN2, each set of training data includes nine groups $\{U_{o\text{avg}}, I_{L\text{avg}}, D, V_{\text{in}}\}$ and corresponding parameters $\{R_L, R_S, V_F\}$.

C. BP-NN Configuration Design

The successful application of BP-NN to the parameter identification of the Buck converter depends not only on the number of training data but also on the configuration of the nonlinear hidden layers and the neurons. Therefore, it is necessary to discuss their influence on BP-NN performance, respectively. To complete the BP-NN configuration design, a closed-loop Buck converter is established in Simulink/MATLAB, and its parameter settings are shown in Table I. The values of parameters $\{R, L, C, R_C, R_L, R_S, V_F\}$ are set within their own aging range and the input voltage V_{in} is set in a wide voltage range of 38–66 V. The switching frequency is 20 kHz. The closed-loop output voltage U_o is set to 24 V. Then, by calling the "sim" function in Simulink, multiple sets of u_o/i_L waveforms will be generated under different parameters, and correspondingly, multiple sets of training data can be collected according to the above section.

First, the number of training data required by BP-NN1 is discussed. Take the BP-NN1 with 1 nonlinear hidden layer and 20 neurons in each layer as an example. As shown in Fig. 9(a), the average relative errors of multiple parameter identification

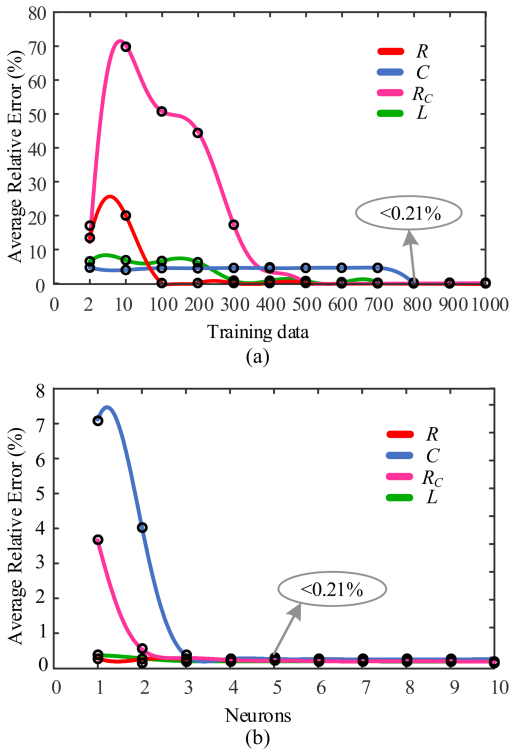

Fig. 9. Relationship between the average relative error and the number of (a) training data and (b) neurons.

are calculated by continuously increasing the number of training data. It can be found that once the number of training data exceeds 800, the average relative error of the load resistance R, the inductance L, the capacitance C, and the parasitic resistance of capacitor R_C decreases to less than 0.21%. Moreover, the influence of different number of neurons on BP-NN1 with 2 hidden layers and 1000 sets of training data is also discussed. After increasing the number of neurons in turn, as shown in Fig. 9(b), the average relative error of the load resistance R, the inductance L, the capacitance C, and the parasitic resistance of capacitor R_C are less than 0.21% when the number of neuron reaches to 5. Similarly, for BP-NN2, only a relatively few number of training data, hidden layers, and neurons are needed to accurately identify parameters $\{R_L, R_S, V_F\}$. Take BP-NN2 with 2 nonlinear hidden layers, 20 neurons per layer, and 5000 sets of training data as an example, the average relative errors of parasitic resistance of inductor R_L, ON-state resistance of MOSFET R_S and the diode forward voltage V_F are 0.30%, 0.32%, and 0.08%, respectively.

From the above discussion, the proposed method not only greatly reduces the number requirements of training data and

TABLE II
COMPONENT PARAMETERS

Component	Value
Input voltage V_{in} (V)	38–66
Switching frequency f_{sw} (kHz)	20
Output voltage U_o (V)	24
Load resistance R (Ω)	15.5
Inductor L (μH)	1712
Capacitor C (μF)	101
Parasitic resistance of output capacitor R_C (Ω)	0.246
Parasitic resistance of inductor R_L (Ω)	0.188
ON-state resistance of MOSFET R_S (Ω)	–
Diode forward voltage V_F (V)	–

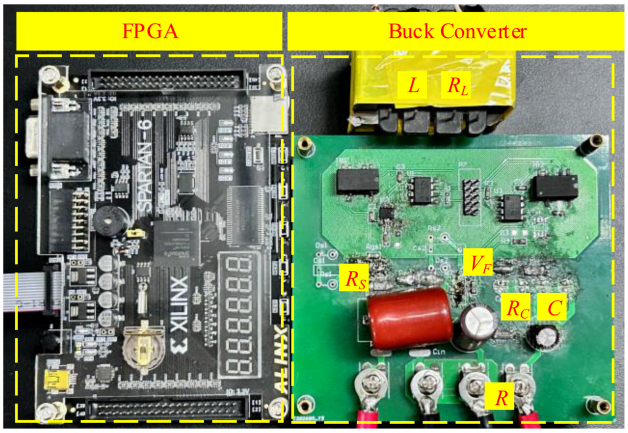

Fig. 10. Experimental setup of physical Buck converter.

TABLE III
OFFLINE MEASURED, BP-NNS IDENTIFICATION, AND IMPROVED BP-NNS IDENTIFICATION OF PARAMETERS

Parameters	R (Ω)	L (μH)	C (μF)	R_C(Ω)	R_L (Ω)	R_S (Ω)	V_F (V)
Offline measured	15.5	1712	101	0.246	0.188	–	–
BP-NNs	15.45	1698	90	0.244	0.092	0.222	0.757
Improved BP-NNs	15.48	1700	102	0.247	0.173	0.124	0.664

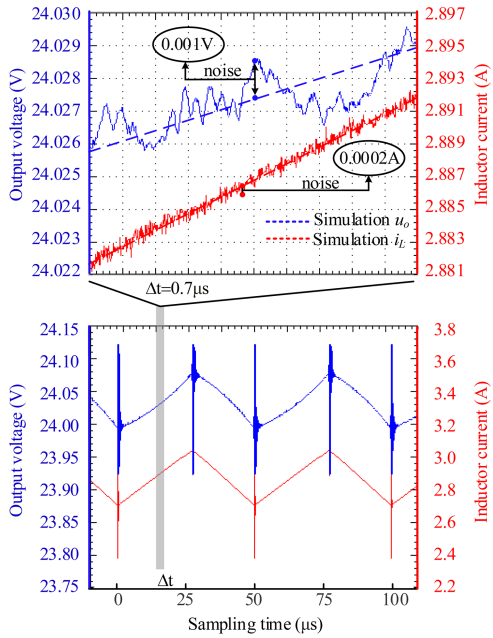

Fig. 11. Output voltage/inductor current waveforms.

neurons, but also has high parameter identification accuracy, as the two explicit time-domain relationships are trained here.

IV. EXPERIMENTAL VERIFICATION

To test the effectiveness of the proposed method in practice, a closed-loop experimental Buck converter with system parameters in Table II is constructed, as shown in Fig. 10. It is noted that the measured values of R_S and V_F are blank because they cannot be directly or accurately measured under offline condition. The ON-state resistance R_S of MOSFET cannot be measured when MOSFET is always OFF under offline conditions, whereas the forward voltage V_F of the diode cannot be accurately measured offline by a multimeter since its conducting current is different from the value under normal operation. It also happens in Tables III, IX, and X. In addition, the NN is constructed by FPGA to complete all the parameter identification. The implementation of the proposed NN in FPGA includes seven submodules, which are data input, data normalization, layer1 calculation, nonlinear activation function implementation, layer2 calculation, antinormalization, and data output. During the implementation of these submodules, most of the logic operations are performed by the adders and multipliers in the FPGA, except for the nonlinear activation function. Since FPGAs are not good at handling nonlinear functions, it is necessary to use the ROM's IP core to create a ROM for storing the quantization data of nonlinear functions.

A. Improved BP-NN Considering the Noise Influence

In practice, the output voltage and inductor current waveforms of the experimental Buck converter under different operating conditions are collected and processed, and then the sampled data are used to identify the component parameters through the above trained BP-NNs. The identification results of parameters $\{R, L, C, R_C, R_L, R_S, V_F\}$ are shown in Table III, from which some parameters have relatively large identification errors, e.g., capacitance C and parasitic resistance of inductor R_L. This is caused by the noise existing in the output voltage and inductor current data sampled from the physical Buck converter, which is not considered in the simulation. Therefore, considering the noise influence in the practice, the above trained BP-NNs should be further improved by adding noise to the training data to achieve better identification accuracy and robustness.

Fig. 11 shows the output voltage and inductor current waveforms of the physical Buck converter under steady-state operating conditions, where there is noise in the range of 0.001 V and 0.0002 A for the output voltage and inductor current in

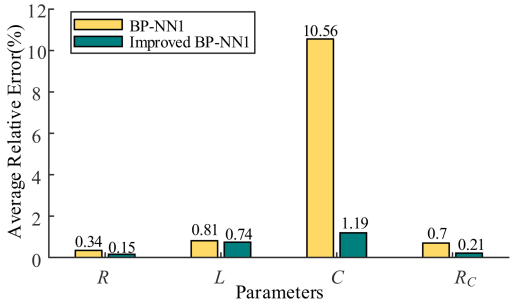

Fig. 12. Parameter identification results of BP-NN1 and improved BP-NN1.

comparison with the simulation data. Therefore, the random values within the above noise range are added to the output voltage and inductor current in the training data of BP-NN1, as shown in the following equation, to simulate the real sampling situation:

$$x_{\text{phys}} = x_{\text{sim}} + x_{\text{nosie}} * (\text{rand} - 0.5) \tag{5}$$

where x_{phy} represents the simulation data with noise, x_{sim} represents the simulation data, x_{noise} represents the added noise, and rand represents a random number from 0 to 1.

Then, BP-NN1 is trained again with the above obtained training data considering practical noise, which is employed to reidentify component parameters. The parameters {R, L, C, R_C} identification results of improved BP-NN1 are shown in Table III. Compared with the original BP-NN1, as shown in Fig. 12, the average relative errors of parameters identification in improved BP-NN1 are basically reduced, especially for the identification of capacitance C. Besides, the relative errors of the load resistance R, the inductance L, the capacitance C, and the parasitic resistance of capacitor R_C are all less than 1.5%. Similarly, a similar improvement is adopted for BP-NN2. The identification results of the parameters {R_L, R_S, V_F} are also shown in Table III. Compared with the original BP-NN2, the parasitic resistance of inductor R_L identified by improved BP-NN2 is closer to the offline measured value. Because the offline measured values of ON-state resistance of MOSFET R_S and diode forward voltage V_F are unknown, their identification improvement cannot be seen directly. This can be further explored through subsequent aging experiments of components. In conclusion, improved BP-NNs can effectively and accurately identify the component parameters of the physical operating Buck converter in operation.

B. Parameter Identification Consistency in Different Operating Conditions

To further verify the stability of the proposed method under different operating conditions, the above improved BP-NN1 has been tested under different input voltage including $V_{\text{in}} = 64$ V, 61 V, 58 V, 55 V, 52 V, 50 V, 46 V, 43 V, and 40 V and loads $R = 8\ \Omega$, 11.7 Ω, and 15.5 Ω. The identified parameters in different operation conditions and offline measured values are summarized in Fig. 13. It can be seen that the estimated values of the inductance L, the capacitance C, the load resistance R, and

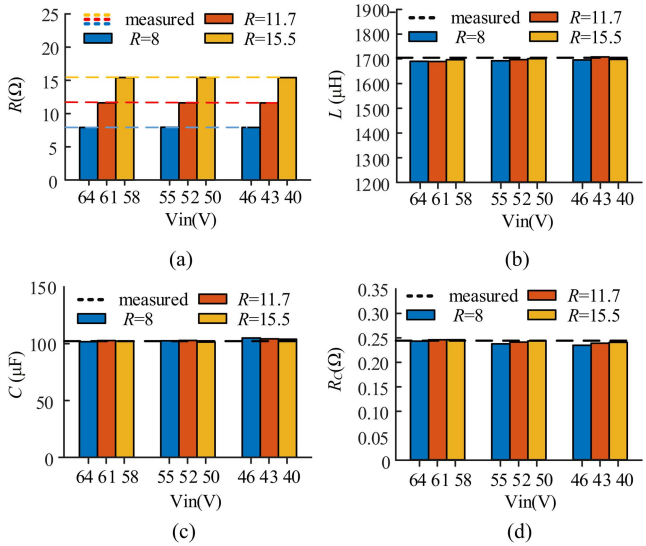

Fig. 13. Estimated parameters under different operating conditions. (a) Load resistance R. (b) Inductance L. (c) Capacitance C. (d) Parasitic resistance of capacitor RC.

the parasitic resistance of capacitor R_C are stable and close to the offline measurements in different loads and input voltages. There is a small difference between the identification results and the offline measured values, which is caused by sampling errors and variations in environmental factors such as temperature.

C. Degradation Monitoring

It is acknowledged that the components suffer from degradation along with the operation of converters. For example, the capacitance may drop by 5%–20% [6] and its corresponding parasitic resistance would increase at the same time. Therefore, during the aging process of these components, it is also important to identify the component parameters smoothly to prevent the risk caused by component failure. To simulate the degradation process of the capacitor in the experiment, four small capacitors are added in parallel with the original capacitor at first and then are taken off one by one. Similarly, the degradation process of the inductor is simulated by sequentially increasing the distance of the air gap four times. In addition, MOSFET, inductor and capacitor are, respectively, in series with additional resistances to simulate the increases of their corresponding parasitic resistances, which are approximately equal to 0.1 Ω each time. Then, both offline measured values and estimated results of different degradation levels are compared in Fig. 14.

As illustrated in Fig. 14(a)–(c), the estimated results of L, C, and R_C are close to the offline measurements overall, which indicates that the proposed method can accurately track degradations of L, C, and R_C. More specifically, the measured and estimated values of L and C are, respectively, shown in Tables IV and V, where L_1 and C_1 represent the initial values. Although the changes are slight, which is only about 5% each time, the accuracy of estimated values can still be ensured that its relative errors are less than 3%. Similarly, the relative errors of R_C are less than 2%, as shown in Table VI.

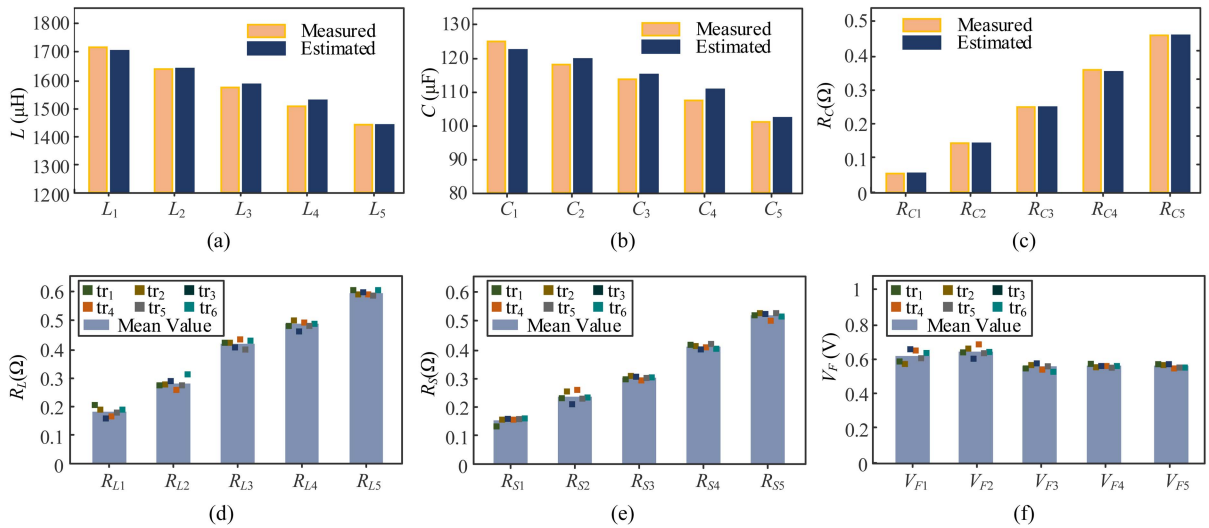

Fig. 14. Degradation process of parameters. (a) Inductance L. (b) Capacitance C. (c) Parasitic resistance of capacitor R_C. (d) Parasitic resistance of inductor R_L. (e) ON-state resistance of MOSFET R_S. (f) Diode forward voltage V_F.

TABLE IV
DEGRADATION PROCESS OF L

Inductance(μH)	Measured value	Estimated value	Relative error
L_1	1712	1700	0.74%
L_2	1635	1639	0.24%
L_3	1570	1581	0.72%
L_4	1504	1527	1.54%
L_5	1439	1438	0.07%

TABLE V
DEGRADATION PROCESS OF C

Capacitance (μF)	Measured value	Estimated value	Relative error
C_1	125	122	2.01%
C_2	118	120	1.62%
C_3	114	115	1.37%
C_4	107	111	2.99%
C_5	101	102	1.19%

TABLE VI
DEGRADATION PROCESS OF R_C

Parasitic resistance of capacitor (Ω)	Measured value	Estimated value	Relative error
R_{C1}	0.054	0.055	1.56%
R_{C2}	0.142	0.144	1.10%
R_{C3}	0.246	0.247	0.21%
R_{C4}	0.354	0.348	1.65%
R_{C5}	0.457	0.454	0.72%

Moreover, the improved BP-NN2 is trained and employed to identify R_L, R_S, and V_F for six times tr_1, tr_2,..., tr_6. The six identification results of R_L, R_S, and V_F, as well as their mean values are illustrated in Fig. 14(d) and (e). In Fig. 14(d) and (e), the results of R_L and R_S fluctuate around the mean value and their identification errors are relatively larger than that of L, C, and $\mathrm{R_C}$, but the aging trend is roughly in line with the increase of 0.1 Ω each time, which indicates that the proposed method can basically track components degradations of R_L and R_S. In addition, the identification results of V_F during the aging processes of R_S are shown in Fig. 14(f). It fluctuates around 0.6 V. In practice, if the value of V_F is measured and known, it can be used as an additional input to retrain improved BP-NN2 to achieve a higher accuracy for the identification of R_L and R_S. Table VII shows the reidentified results of R_L with V_F measured as 0.6 V. The relative errors of R_L are all less than 5% during the whole simulated degradation process. On the other hand, because the ON-state resistance of MOSFET R_S cannot be measured offline, Table VIII shows the identification results of increment ΔR_S, whose relative errors are less than 3%.

TABLE VII
DEGRADATION PROCESS OF R_L

Parasitic resistance of inductor (Ω)	Measured value	Estimated value	Relative error
R_{L1}	0.188	0.179	4.86%
R_{L2}	0.276	0.275	0.19%
R_{L3}	0.380	0.371	2.48%
R_{L4}	0.487	0.501	2.88%
R_{L5}	0.588	0.601	2.24%

TABLE VIII
DEGRADATION PROCESS OF R_S

Increment (Ω)	Measured value	Calculated value	Relative error
ΔR_{S1}	0.088	0.085	2.29%
ΔR_{S2}	0.192	0.190	0.98%
ΔR_{S3}	0.299	0.307	2.42%
ΔR_{S4}	0.400	0.408	1.89%

Furthermore, the time required for completing the whole parameter identification is about 28 μs. Among them, the identification time of inductance L is 5.8 μs, capacitance C is 6.23 μs, load resistance R is 5.3 μs, parasitic resistance of capacitance R_C is 6.75 μs, parasitic resistance of inductor R_L, ON-state resistance of MOSFET R_S, and diode forward voltage V_F is 4.75 μs. Therefore, the parameter identification can be completed fast.

TABLE IX
COMPONENT PARAMETERS

Component	Value
Input voltage V_{in} (V)	38–66
Switching frequency f_{sw} (kHz)	100
Output voltage U_o (V)	24
Load resistance R (Ω)	16.4
Inductor L (μH)	255.88
Capacitor C (μF)	25.16
Parasitic resistance of output capacitor R_C (Ω)	0.298
Parasitic resistance of inductor R_L (Ω)	0.044
ON-state resistance of MOSFET R_S (Ω)	–
Diode forward voltage V_F (V)	–

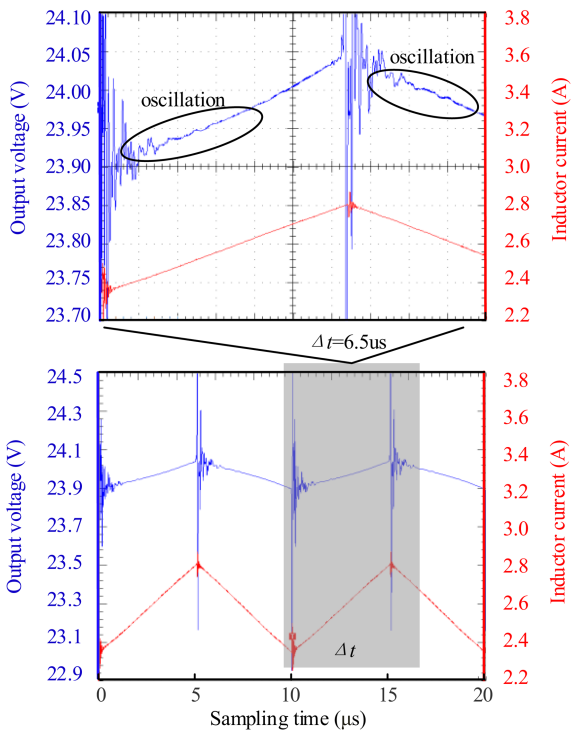

Fig. 15. Output voltage/inductor current waveforms under 100-kHz operating conditions.

D. Validation at Higher Frequency

The proposed method is also applicable to the Buck converter working under a higher switching frequency. However, it is noteworthy that the higher the switching frequency is, the noise interference on the sampled data caused by the switching process is more severe, which may be adverse to the identification accuracy.

In this section, a 100-kHz Buck converter is redesigned with parameters in Table IX. Its steady-state output voltage and inductor current waveforms are shown in Fig. 15, where the output voltage oscillates for a long time resulting from the hard-switching operation. The data in the oscillation period are commonly discarded, and then the sampling rate is required to be higher to obtain six points from the remaining common region,

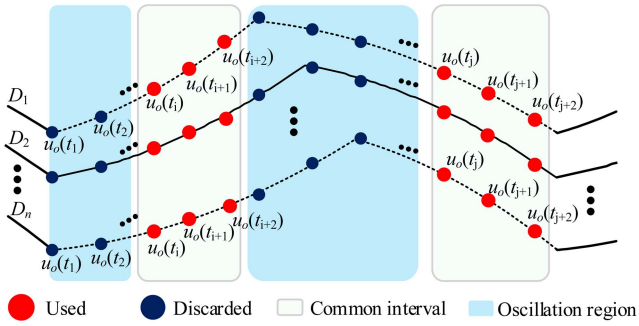

Fig. 16. Sampling strategy of instantaneous values at different duty cycles.

TABLE X
OFFLINE MEASURED AND BP-NNS IDENTIFICATION OF PARAMETERS

Parameters	R (Ω)	L (μH)	C (μF)	R_C (Ω)	R_L (Ω)	R_S (Ω)	V_F (V)
Offline Measured	16.4	255.88	25.16	0.298	0.044	–	–
BP-NNs	16.34	257.67	26.24	0.303	0.042	0.107	0.6
Relative error	0.35%	0.70%	4.29%	1.85%	4.54%		

as demonstrated in Fig. 16. Finally, the results of parameter identification are shown in Table X. Compared with the identification results under 20 kHz, it can be found that the identification error is a little increased under 100 kHz, which is in coincidence with the deteriorated noise interference. Nevertheless, the identification error is still small and hence the proposed method is also applicable to identify component parameters for the Buck converter under higher switching frequency.

E. Comparison

Finally, a comparative analysis between the proposed method and other methods listed in Fig. 1 is shown in Table XI, including topology, switching frequency, main measured variables, the number of parameter identifications, implementation, relationship, speed, and error.

As summarized in Table XI, the target converter to be identified mainly concentrates on Buck and Boost converters, which operate under tens of kHz. Parameters of a single component are identified with a specific frequency component extraction method in [8] and [9], which extracts the peak values or RMS values of measured variables to identify the health indicators of the capacitor. Moreover, the circuit model-based method in [10] and [11] uses the existing voltage/current data to calculate the value of ESR or C in the Boost converter, which does not need additional sensors and filters. The above two methods cannot identify parameters for multiple components at the same time, which are improved in [15], [21], and [27]. In [15], multiple components' parameters are solved from the transfer function between the output voltage and duty cycle. However, it needs the injection of PRBS, which will be detrimental to the system stability. To avoid this shortcoming, Peng et al. [21] established a digital twin and updated its parameters iteratively until it

TABLE XI
COMPARISON OF PARAMETER IDENTIFICATION METHOD

Method	Topology	Switching Frequency	Main Measured Variables	Number of Parameter Identification	Implementation	Relationship	Speed	Error
Specific Frequency Component Extraction Method [8] , [9]	Three-phase Inverter [8] Boost[9]	2.5 kHz [8] 10 kHz [9]	Peak values of V_{C_3fSW} and I_{C_3fSw} [8] RMS values of V_{PV} and I_C [9]	Single	Extra Filters and Detectors	Explicit	Medium	C: 2.1%–3.9% [8] Z_C: 0.03%–0.34% [9]
Circuit model–based Method [10] ,[11]	Boost [10] ,[11]	10 kHz [10] 50 kHz [11]	Peak values of V_{PV} and I_{PV} [10] Instantaneous value of v_{dc} ,v_S *and* i_L [11]	Single	Simple	Explicit	Fast	ESR: 0.1%–6.1% [10] C: <3.5% [11]
System Identification [15]	Buck	20 kHz	300 instantaneous value of v_O in multiple cycles	Multiple	Extra PRBS Injection	Explicit	Medium	C: 1.2%–18% L: 5.4%–9.5% R_C: 0.4%–10.8%
Digital Twin Based Method [21]	Buck	20 kHz	Instantaneous values of v_O *and* i_L in multiple cycles	Multiple	Simple	Explicit	Slow	C:10.3% Others: not mentioned
NN-based Method [27]	Buck	40 kHz	200 instantaneous value of v_O in multiple cycles	Multiple	Additional Signal Processing	Ambiguous	Fast	C: average 2.08% R_C: average 2.65% L: average 2.42% R_L: average 2.88%
Proposed NN -based Method	Buck	20 kHz	10 instantaneous value of v_O *and* i_L in one cycle	Multiple	Simple	Explicit	Fast	R: average 0.15% C: average 1.83% R_C: average 1.05% L: average 0.66% R_L: average 2.53% ΔR_S: average 1.89%

approached the physical converter. However, the identification process takes a long time because the PSO algorithm is employed to search the parameter. On the other hand, an NN is employed in [27] to fit the relationship between the frequency domain features as well as time domain statistical features of output voltage and component parameters. Then, parameter identification can be completed quickly. However, the ambiguous relationship limits parameter identification accuracy. In addition, the feature acquisition also requires a large amount of sampling data and complex processing. In this article, an NN is used to fit the explicit relationships between the component parameters and voltage/current in the Buck converter, and hence multiple component parameters can be simultaneously identified with fast speed and high accuracy. Moreover, measured variables in one switching cycle and relatively few sampled points are needed in the proposed method. Besides, no additional signal processing is needed, which is simple to implement. From Table XI, the average identification error is improved in the proposed method than other methods in general.

V. CONCLUSION

In this article, a full-parameter identification method of Buck converter through BP-NN fitting explicit time-domain relationships is proposed. Thanks to the explicit time-domain relationships between the instantaneous/average values of output voltage/inductor current and component parameters, only a relatively small amount of training data, hidden layers, and nodes are demanded to construct BP-NNs. The average relative errors of all parameter identification results using ideal simulation data are less than 0.4%. Moreover, considering the practical sampling noise of the experimental closed-loop Buck converter, the trained BP-NNs are further improved, which retains high parameter identification accuracy in different operating conditions and component degradations. Therefore, due to the favorable advantage of simple implementation and high accuracy, the proposed method is attractive in the condition monitoring of various converters, as long as their explicit time-domain relationship are revealed.

REFERENCES

[1] V. Madonna, P. Giangrande, and M. Galea, "Electrical power generation in aircraft: Review, challenges, and opportunities," *IEEE Trans. Transp. Electrific.*, vol. 4, no. 3, pp. 646–659, Sep. 2018.
[2] S. S. Williamson, A. K. Rathore, and F. Musavi, "Industrial electronics for electric transportation: Current state-of-the-art and future challenges," *IEEE Trans. Ind. Electron.*, vol. 62, no. 5, pp. 3021–3032, May 2015.
[3] P. T. Krein, "Data center challenges and their power electronics," *CPSS Trans. Power Electron. Appl.*, vol. 2, no. 1, pp. 39–46, Mar. 2017.
[4] S. Yang, D. Xiang, A. Bryant, P. Mawby, L. Ran, and P. Tavner, "Condition monitoring for device reliability in power electronic converters: A review," *IEEE Trans. Power Electron.*, vol. 25, no. 11, pp. 2734–2752, Nov. 2010.
[5] S. S. Manohar, A. Sahoo, A. Subramaniam, and S. K. Panda, "Condition monitoring of power electronic converters in power plants – A review," in *Proc. 20th Int. Conf. Elect. Mach. Syst.*, 2017, pp. 1–5.
[6] H. Soliman, H. Wang, and F. Blaabjerg, "A review of the condition monitoring of capacitors in power electronic converters," *IEEE Trans. Ind. Appl.*, vol. 52, no. 6, pp. 4976–4989, Nov./Dec. 2016.
[7] Y. Wu, Y. Wang, Y. Jiang, and Q. Sun, "Multiple parametric faults diagnosis for power electronic circuits based on hybrid bond graph and genetic algorithm," *Measurement*, vol. 92, pp. 365–381, Oct. 2016.
[8] P. Sundararajan, M. H. M. Sathik, F. Sasongko, C. S. Tan, M. Tariq, and R. Simanjorang, "Online condition monitoring system for dc-link capacitor in industrial power converters," *IEEE Trans. Ind. Appl.*, vol. 54, no. 5, pp. 4775–4785, Sep./Oct. 2018.

[9] M. W. Ahmad, N. Agarwal, P. N. Kumar, and S. Anand, "Low-frequency impedance monitoring and corresponding failure criteria for aluminum electrolytic capacitors," *IEEE Trans. Ind. Electron.*, vol. 64, no. 7, pp. 5657–5666, Jul. 2017.
[10] M. W. Ahmad, N. Agarwal, and S. Anand, "Online monitoring technique for aluminum electrolytic capacitor in solar PV-based dc system," *IEEE Trans. Ind. Electron.*, vol. 63, no. 11, pp. 7059–7066, Nov. 2016.
[11] Z. Zhao, P. Davari, W. Lu, and F. Blaabjerg, "Online dc-link capacitance monitoring for digital-controlled boost PFC converters without additional sampling devices," *IEEE Trans. Ind. Electron.*, vol. 70, no. 1, pp. 907–920, Jan. 2023.
[12] Y. Peng and H. Wang, "Duty cycle based condition monitoring of MOSFETs in digitally-controlled dc-dc converters," in *Proc. IEEE Appl. Power Electron. Conf. Expo.*, 2020, pp. 364–369.
[13] S. Dusmez, M. Bhardwaj, L. Sun, and B. Akin, "In situ condition monitoring of high-voltage discrete power MOSFET in boost converter through software frequency response analysis," *IEEE Trans. Ind. Electron.*, vol. 63, no. 12, pp. 7693–7702, Dec. 2016.
[14] M. Algreer, M. Armstrong, and D. Giaouris, "Active online system identification of switch mode dc–dc power converter based on efficient recursive DCD-IIR adaptive filter," *IEEE Trans. Power Electron.*, vol. 27, no. 11, pp. 4425–4435, Nov. 2012.
[15] B. X. Li and K. S. Low, "Low sampling rate online parameters monitoring of dc–dc converters for predictive-maintenance using biogeography-based optimization," *IEEE Trans. Power Electron.*, vol. 31, no. 4, pp. 2870–2879, Apr. 2016.
[16] C. Wang, M. Armstrong, S. Gadoue, and P. Missailidis, "System identification of a dc-dc converter system using a fast affine projection algorithm," in *Proc. 7th IET Int. Conf. Power Electron., Mach. Drives*, 2014, pp. 1–6.
[17] M. Ahmeid, M. Armstrong, S. Gadoue, M. Al-Greer, and P. Missailidis, "Real-time parameter estimation of dc–dc converters using a self-tuned Kalman filter," *IEEE Trans. Power Electron.*, vol. 32, no. 7, pp. 5666–5674, Jul. 2017.
[18] Z. Cen and P. Stewart, "Condition parameter estimation for photovoltaic buck converters based on adaptive model observers," *IEEE Trans. Rel.*, vol. 66, no. 1, pp. 148–160, Mar. 2017.
[19] J. Poon, P. Jain, C. Spanos, S. K. Panda, and S. R. Sanders, "Fault prognosis for power electronics systems using adaptive parameter identification," *IEEE Trans. Ind. Appl.*, vol. 53, no. 3, pp. 2862–2870, May/Jun. 2017.
[20] Y. Peng and H. Wang, "Application of digital twin concept in condition monitoring for dc-dc converter," in *Proc. IEEE Energy Convers. Congr. Expo.*, 2019, pp. 2199–2204.
[21] Y. Peng, S. Zhao, and H. Wang, "A digital twin based estimation method for health indicators of dc–dc converters," *IEEE Trans. Power Electron.*, vol. 36, no. 2, pp. 2105–2118, Feb. 2021.
[22] Y. Liu, G. Chen, Y. Liu, L. Mo, and X. Qing, "Condition monitoring of power electronics converters based on digital twin," in *Proc. IEEE 3rd Int. Conf. Circuits Syst.*, 2021, pp. 190–195.
[23] S. Chen, S. Wang, P. Wen, and S. Zhao, "Digital twin for degradation parameters identification of dc-dc converters based on Bayesian optimization," in *Proc. IEEE Int. Conf. Prognostics Health Manage.*, 2021, pp. 1–9.
[24] G. Rojas-Dueñas, J. R. Riba, and M. Moreno-Eguilaz, "Nonlinear least squares optimization for parametric identification of dc–dc converters," *IEEE Trans. Power Electron.*, vol. 36, no. 1, pp. 654–661, Jan. 2021.
[25] S. Zhao, Y. Peng, Y. Zhang, and H. Wang, "Parameter estimation of power electronic converters with physics-informed machine learning," *IEEE Trans. Power Electron.*, vol. 37, no. 10, pp. 11567–11578, Oct. 2022.
[26] B. H. Lin, J. T. Tsai, and K. L. Lian, "A non-invasive method for estimating circuit and control parameters of voltage source converters," *IEEE Trans. Circuits Syst. I, Reg. Papers*, vol. 66, no. 12, pp. 4911–4921, Dec. 2019.
[27] Y. Jiang, Y. Liu, and Z. Yang, "Parameter identification of dc–dc converter based on dendrite net under fluctuating input voltages," *IET Power Electron.*, vol. 16, no. 12, pp. 2076–2090, Sep. 2023.
[28] R. Leyva, L. Martinez-Salamero, B. Jammes, J. C. Marpinard, and F. Guinjoan, "Identification and control of power converters by means of neural networks," *IEEE Trans. Circuits Syst. I, Fundam. Theory Appl.*, vol. 44, no. 8, pp. 735–742, Aug. 1997.
[29] T. L. Daniel and D. L. Chantal, "Neural networks," in *Discovering Knowledge in Data: An Introduction to Data Mining*. Hoboken, NJ, USA: Wiley, 2014, pp. 187–208.
[30] C. C. Aggarwal, *Neural Networks and Deep Learning*. Berlin, Germany: Springer-Verlag, 2018.

Zhennan She received the B.E.E. degree in electrical engineering and automation in 2021 from Xiamen University, Xiamen, China, where he is currently working toward the master's degree in electrical engineering with the School of Aerospace Engineering.

His research interests include neural network–based condition monitoring of power electronics converters and their hardware implementation.

Yisi Liu received the B.E.E. and M.S. degrees in electrical engineering from the School of Aerospace Engineering, Xiamen University, Xiamen, China, in 2020 and 2023, respectively. He is currently working toward the Ph.D. degree in electrical engineering with Electrical Energy Management Group Laboratory, Department of Electrical and Electronic Engineering, University of Bristol, Bristol, U.K.

His research interests include condition monitoring of power electronic converters and the reliability analysis of wide-bandgap power semiconductor devices.

Wen Cao received the B.E.E. degree in electric engineering from Jimei University, Xiamen, China, in 2023. She is currently working toward the M.S. degree in electrical engineering with the School of Aerospace Engineering, Xiamen University, Xiamen, China.

Her current research interest focuses on the analysis of system operation following dc microgrids short-circuit faults.

Guipeng Chen received the B.E.E. and Ph.D. degrees in electrical engineering from Zhejiang University, Hangzhou, China, in 2011 and 2017, respectively.

From 2017 to 2019, he was a postdoctoral Researcher and afterwards an Associate Professor with the Department of Instrumental and Electrical Engineering, Xiamen University, Xiamen, China. He authored or coauthored more than 60 technical papers. His research interests include graph theory-based automatic topology derivation and digital twin-based condition monitoring of power electronics converters.